# Surface area and pore-size distribution in clays and shales

Utpalendu Kuila and Manika Prasad: Colorado School of Mines

## Abstract

One of the biggest challenges in estimating transport and storage properties of shales is a lack of understanding of their complete pore size distributions. Shale matrix has predominantly micro (pores less than 2 nm diameter) to meso-pores (pores with 2-50 nm diameter). These small pores in shale matrix are mainly associated with clay minerals and organic matter. Thus, comprehending the controls of clays and organic matter on the pore-size distribution is critical to understanding the shale pore network. Historically mercury intrusion techniques are used for pore-size analysis of conventional reservoirs. However, for unconventional shale reservoirs, very high pressures (> 60,000 psi) would be required for mercury to access the full pore-structure which has potential pitfalls. Nitrogen gas adsorption techniques can be used to characterize materials dominated by micro and mesopores (2-50 nm). A limitiation of this techniques is that it fails to measure large pores (diameter >300 nm). In this study, we have used a combination of nitrogen gas adsorption and mercury intrusion to study the spectrum of pore-sizes in shales and clays.

Our results on pure clay minerals show that (i) clays have a mulit-scale pore-structure at different dimensions, (ii) Micropores are associated with montmorillonite clays but not with kaolinite, (iii) compaction results in decrease in pore volume and reduction of pore-size in the macropores of the clays while the micropores are shielded from the effect of compaction, and (iv) in natural shales, mineralogy controls the pore-size distributions for shales and presence of micropores in natural shales can be correlated with the dominance of illite-smectite type of clays in the rock.

## Introduction

Over the past decade, interest in shale reservoirs increased due to commercial success of gas-shale plays. In contrast to conventional plays, these plays typically have very fine-grained rock texture (dominant grain size ≤62.5 μm), low porosity (≤10%) and very low permeabilities (in nanodarcy range). These are source rocks with high organic content (≥2% weight fraction **T**otal **O**rganic **C**arbon, TOC) that also function as reservoir rocks. Gas reserves in these plays are huge, estimated to be ~1000 TCF in North America and ~200 TCF in Europe (Jaffe, 2010). A recent U.S. Energy Information Administration (EIA) report states that in the US, natural gas production from shales will triple to 4.2 TCF by the year 2030, making it about 18% of total US natural gas production. Despite the commercial importance of shale formations, their physical properties especially porosity and pore-size distributions are still poorly understood.

Porosity measurements in shales are complicated because of the very fine-grained texture, small pore sizes, extremely low permeability, and the strong interaction of water with clay minerals, which are often the major component in these rock types. Shales exhibit dual-porosity structure and have a more complex pore-structure than the sandstones and limestones. One of the biggest challenges in estimating transport and storage properties of shales has been a lack of understanding of their complete pore size distributions. In gas shale plays, gas flow occurs mainly through the interconnected fracture network system. This fracture network system is postulated to be recharged by gas flowing through the shale matrix dominated by micropores (pores smaller than 2 nm as per IUPAC classification) to mesopores (pore-size from 2nm to 50 nm as per IUPAC classification)[*]. Gas flow in the nanoporous shale matrix is expected to be a combination of Knudsen diffusion and slip flow in nanometer-sized pores and Darcy-like flow in micrometer-or larger size pores. Modeling this flow requires knowledge about the pore-radius and pore-size distribution. Historically, mercury intrusion techniques are used for pore-size analysis of conventional reservoirs. However, for unconventional shale reservoirs, very high pressures (> 60,000 psi) would be required for mercury to access the full pore-structure. Bustin et al. (2008) pointed out potential pitfalls of using very high mercury injection pressures to get the pore size distribution in shales. Compressibility of the rock structure, possibility of breaking the particles, and opening closed pores will affect the data collected at such high pressures. Gas adsorption techniques are widely used in the chemical, ceramic, and pharmaceutical industry to characterize the pore-structure and surface areas of powders

and fine microporous materials such as activated carbon, carbon nanotubes, zeolites and catalysts. Different gases such as nitrogen, argon and carbon dioxide are used to investigate very fine pores in the range of 0.3 nm – 100 nm.  Nitrogen is the most widely used gas for such experiements, and it works well for materials dominated by mesopores (2-50 nm).  A limitiation of this techniques is that it fails to measure large pores (diameter >300 nm). A combination of mercury intrusion and nitrogen gas adsorption gives us the entire pore-size distribution.

The extremely small pores in shale matrix are mainly associated with clay minerals and organic matter. Comprehending the controls of clays and organic matter on the pore-size distribution is critical to understand the shale pore network. Several authors have reported associated microporosity with clays. Advanced imaging techniques reveal small pore structure of nanometer scale in clays and kerogen with in shales (for example, Javadpour, 2009). In this paper, we will present pore-size distribution results obtained from nitrogen gas-adsorption and mercury intrusion studies on clays and natural shales. We will discuss the implications and controls that end-members like clays exert on pore-size distributions of natural shales and what effects these pore-size distributions can have on their physical physical properties.

*Note that in this paper, we use the International Union of Pure and Applied Chemistry (IUPAC) pore-size classification that classifies micropores as pores below 2 nm and mesopores as pores between 2nm to 50 nm (Sing, 1985).

## Previous studies

A unique feature of shale rocks is their extremely small pore-sizes that can be attributed to their fine-grained nature. In the literature, a wide variety of terminology is used to classify small pores (for example, nanopore, mesopore, micropores). The International Union of Pure and Applied Chemistry (IUPAC) has recommended the following classification of pores according to their width, that is, diameter of a cylindrical pore, distance between two sides of a slit-shaped pore, or the smallest dimension in irregular pore (pore-throat):

1. Micropores: pores with pore-width below 2 nm
2. Mesopores: Pores with pore-width between 2nm to 50 nm
3. Macropores: Pores with pore-width greater than 50 nm

The advantage of this classification is that it is based on the physics of physisorption of nitrogen isothermal adsorption at 77.3K and 1 atmosphere pressure in various pore types. Different mechanisms, such as, multilayer adsorption, capillary condensation, and micropore filling predominate in macropores, mesopores, and micropores, respectively. Its disadvantage is that the classification is not intuitive; nano-sized pores are termed as micro- and mesopores. Additionally, pores larger than 50 nm are not subdivided further. They are jointly classified as macropores. However, since the IUPAC classification (Sing 1985) is a non-arbitrary classification, we will use the IUPAC pore-size classification for this paper. The IUPAC classification is more appropriate for shales since we expect shales to have a considerable volume of their pore space in nanometer-sized pores. For future work, we recommend defining a pore size classification that is more appropriate for reservoir rocks.

Shale matrix has predominantly micro to meso-pores. The presence of these extremely small pores (generally associated with clays and the kerogen) has been documented in several studies. Diamond (1970) reported pore-size distribution of clays using Hg-porosimetry technique. Rutherford et al. (1997) studied pure homoionic clays with $N_2$ and neo-hexane adsorption techniques and reported presence of 14-66% micropores of the total pore volume depending upon the cation. Connell-Madore and Katsube (2006) reported pore-size distribution for shales from Beaufort-MacKenzie Basin and Scotian shelf using Hg-porosimetry technique. They reported unimodal pore size distribution that decreases with compaction with the modal size between 25 nm - 10 μm range at shallow burial depth and between 2.5 - 25 nm range at deep burial. Ewy and Morton (2009) also reported bimodal to unimodal pore-size distributions from Hg-porosimetry techniques on artificial shale pellets compacted in the laboratory. Most pore-size distribution studies on shales use Hg porosimetry. Bustin et al. (2008) recommend using a combination of gas-adsorption and Hg-porosimetry for shales due to problems associated with high-pressure mercury intrusion to capture small pores. They reported bimodal size distributions with modes around 10 nm and the other around 10,000 nm for a Barnett and an Antrim formation shale using a combination of Hg porosimetry, $N_2$ and $CO_2$ adsorption techniques. The controls on pore-structures of shales exerted by the pore-structure charateristics of their end-members such as like clay and organic matter have not been extensively researched. Ross and Bustin (2009) studied the pore-structure of Devonian-Missisipian and of Jurrasic shales from Western Canadian Sedimentary Basin using the combined technique. They report good correlation between micropore volumes and TOC content of organic rich shales, a positive correlation between clay content and total Hg-porosity, and a systematic change in pore structure with increasing clays. More recently, advanced imaging techniques have allowed imaging of small pore structure of nanometer scale in clays and kerogen.  Javadpour (2009) used Atomic Force Microscope to show pores and grooves with dimensions about few nanometers associated with clays. Loucks et al. (2009) showed back-scattered SEM images of nanometer-scale pore associated with clays and kerogen in Barnett shale and revealed pores as small as 4 nm. These studies suggest that the small pores in shales are associated with clays and kerogen. A systematic study of characterizing the pore-structures of shale end members such as clay minerals, clay-sized fractions, and kerogen and of analyzing the controls exerted these end-members on physical properties of natural shales is still lacking. This study focuses on understanding pore size distributions in different clay mineral as powders and as compacted samples and on comparing these end-member results with pore-size distributions in natural shales.

## Theoretical Consideration:

Surface area and pore-size distributions are important textural parameters to understand the gas-adsorption capacities and gas-flow mechanisms in shales. Gas in shale plays are present either as free gas compressed in the pores or as adsorbed gas on the surface of the pores. The sorbed gas capacity is typically correlated with abundance, maturity and type of kerogen present in shales. Bustin et al. (2008) pointed out the importance of presence of micropores associated with clays and kerogen to the gas-adsorption potential of shales. The surface area-to-pore volume increases exponentially with decreasing pore-sizes and increasing surface areas, and hence the ratio of adsorbed gas to compressed free gas increases inversely related to pore-size. Knowledge about the surface area, micropore volumes and the total pore-size distribution is critical in understanding the gas-in-place for these plays. Gas flow in the shale matrix is expected to be a combination of Knudsen diffusion and slip flow in the nanopores and Darcy-like flow in the larger pores. Modeling this flow requires knowledge about the pore-radius and pore-size distribution.

Gas-adsorption experiments are used to obtain information about surface areas, micropore volumes and pore-size distributions for pores with diameter less than 100 nm. In the section, we will discuss the different techniques used to estimate these parameters from gas-adsorption isotherms. In a gas adsorption experiment, a de-gassed sample is exposed to nitrogen gas near cryogenic temperature (-197.3 $^{o}$C) at a series of precisely controlled pressures. Nitrogen adsorption volumes are measured over the relative equilibrium adsorption pressure ($P/P_o$) range of 0.05 -1.0, where $P_o$ is the condensation pressure of nitrogen at laboratory conditions. The gas adsorption isotherm is reported as the volume of gas adsorbed as a function of $P/P_o$. At $P/P_o$ equal to 1, the entire gas is condensed to liquid inside the pores. Desorption experiment is carried by systematically reducing the pressure from the condensation pressure $P_o$ resulting in liberation of the adsorbed gas molecules. As with the adsorption process, the changing volume of gas on the solid surface is quantified and reported as the desorption isotherm. The shape of the isotherm and the hysteresis is used to qualitatively predict the types of pores present in the samples. IUPAC (Sing 1985) classifies the adsorption isotherms into six types, Type I to Type VI and the hysteresis patterns into four types, Type H1 to Type H4. Details about the various isotherm types are given in Sing, 1985.

The surface area of the samples is calculated by applying BET theory to the gas adsorption data. BET theory suggests that there is a decrease in enthalpy of the adsorption from the first layer (monolayer) to subsequent layers. The method uses a transform plot to determine the amount of nitrogen required to cover the total surface area accessible to gas molecules, i.e. external surface area, and the surface area caused by micro-, meso-, and macropores with a complete monolayer of nitrogen. The monolayer capacity is calculated from the adsorption isotherm and the monolayer capacity is converted into specific surface area (surface area per unit gram) by assessing the average area occupied by each molecule in complete monolayer. ISO 9277:2010 suggests using 16.2 nm$^2$ as the molecular cross-sectional area of nitrogen at 77.3 K. The BET plots generally show linear trend with positive intercept over the approximate P/Po range of 0.05 to 0.30. The BET theory works best for nonporous, mesoporous (dominated by mesopore with 2-50 nm pore width) and macroporous materials and is theoretically not applicable for micropores (<2nm pore width) because of occurrence of micropore filling instead of multilayer adsorption. In materials containing micropores, it is difficult to seperate between micropore filling and the multilayer adsorption processes. Nevertheless, BET surface area has been used on adsorption isotherms from materials containing micropores to quantify surface area. ISO 9277:2010 also suggests using BET method to quantify surface area for materials with micropores but using the reported value with caution: such values should not be used as true surface area but should be considered as equivalent BET area. The best indicator of presence of micropores is the negative values of the intercept on the ordinate of BET plot. ISO 9277:2010 suggests a procedure to modify the BET method if presence of micropore is detected, which has been followed during our analysis.

t-plot is a technique used widely to estimate the micropore volume and 'the open surface area', the surface area from mesopores, macropores, and external surface area (that is the total surface area excluding the surface area of micropores). In t-plots, the adsorbed $N_2$ volume ($V_a$) is plotted against statistical thickness (t) of the adsorbed layer of $N_2$. Several thickness equations are available in the literature. In this study, the universal t-curve of $N_2$ of Harkins-Jura (Webb and Orr, 1997) is used:

$$t = [13.99/(0.034 - \log(P/P_o))]^{0.5},$$

where t is the statistical thickness (t) of the adsorbed layer of N2 in Å. Figure 1 shows idealized examples of t-plots for a microporous solid and for a sample free of micropores (Webb and Orr,1997). If the Va vs t plot yields a straight line that passes through the origin, then the sample is considered to be free of micropores. t-plot of microporus material shows a straight line at high t and a convave-down curve at low t. Extrapolation of the linear region to the Va axis gives the micropore volume and the slope of the linear fit gives 'the open surface area'.

The pore size distribution from gas adsorption is obtained using Barett-Joyner-Halenda (BJH) method. This theory uses Kelvin equation relating the radius of the liquid-vapour meniscus with the vapour pressure during capillary condensation through cylindrical pores. The BJH theory uses Kelvin equation and incorporates the effect of thinning of adsorbed layer through thickness curves. The most generally applied thickness curves are those of Harkin-Jura and Halsey (Webb and Orr, 1997). In this paper, the Halsey thickness curves are used. At pressure Po (condensation pressure), the pores are completely filled with the condensed adsorptive (in liquid state). The BJH method involves an 'imaginary emptying of condensed adsorptive' as the relative pressure is decreased (Webb and Orr, 1997) and liquid evaporates out from the larger pore, as

described by Kelvin equation and larger radius of meniscus. Even though theoretically the BJH method is a desorptive method, it can be used for following both the adsorption isotherm, downward from high to low relative pressure, or the desorption curve. However, pore-size distribution obtained from desorption curve shows a peak around 4 nm, which is an artefact due to tensile strength effect (TSE) phenomena (Groen et al., 2003). In this study, we report the pore-size distribution obtained by applying BJH method from the adsorption isotherm.
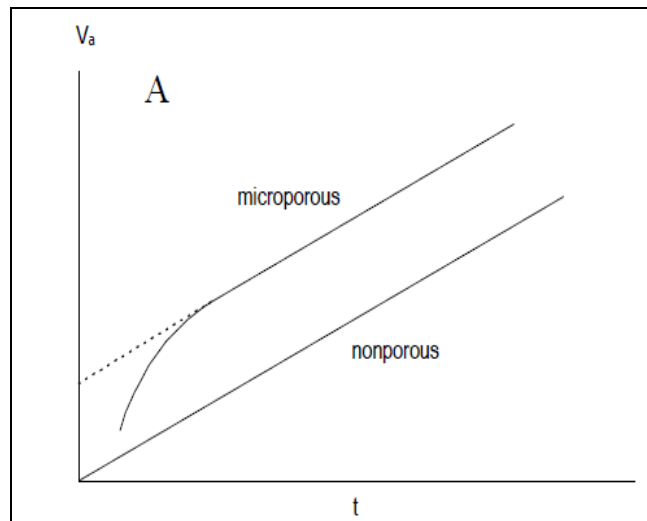


**Figure 1: Schematic example of t-plots for two samples with and without micropores taken from Webb and Orr, 1997. The sample free of micropore (referred as nonporous) shows a linear fit that passes through the origin. Microporous samples shows straight line at at high t and a convave-down curve at low t. The intercept on the y-axis gives a measure of the micropores.**

## Methods and Materials:

### Materials

Wyoming montmorillonite (Swy-2) and low-defect Georgia kaolinite (KGa-1b) were obtained from the Source Clay Repository of Clay Mineral Society. These are natural samples and so have some contaminants but they are dominated by the specified minerals. Wyoming montmorillonite powder (Swy-2) was artificially compacted using cold pressing techniques to make pellets. The pressure was increased at a very slow rate. The powdered samples were put inside a one-and-half inch cylindrical barrel and then pressure was increased at a very slow rate. The inner surfaces of the barrels were coated with Teflon tapes to prevent sticking of charged clays with the walls during the pressing. This also helps in reducing the friction associated while pushing the sample out of the barrel and sample recovery was made simple. Samples samples were prepared by pressing at different pressures (between 6000 psi to 14000 psi) to obtain pellets with different porosities. The pellets were named using clay mineral identifier and the pressure applied, e.g. sample Mont-6K means the pellet is made from Wyoming Montmorillonite by applying 6000 psi of axial load. Rectangular chips (about 0.5 g in weight) were cut from the pellets using a diamond saw for the gas adsorption experiments.

Shale samples from two different locations were also tested. An illite-rich Cambrian shale sample from Silver Hill, Montana was obtained as ground rock chips from the Clay Mineral society. This particular shale is used as the source clay for illitic clays. The second shale samples analyzed was the Niobrara marl B-C obtained from core of the Niobrara Formation in the Berthoud State No. 3 well, Berthoud Field, Larimer County, Colorado (Pollastro, 1992). The cores were cut into small chips (each weighing from 200-500 mg) from the cores. Niobrara is mainly calcitic with some amounts of illite-smectite clays (Pollastro, 1992) while the Cambrian shale has dominant silt mineralogy with significant amount of illitic clays (Srodon and Eberl, 1984).

### Gas Adsorption Experiment:

The gas adsorption experiment using nitrogen as the adsorbent is conducted on Micromeritics ASAP 2020 surface area analyzer, which uses a static volumetric method for measuring the amount of adsorbed gas. Sample preparation was carried out in accordance to ISO 9277: 2010. Sample was degassed at $200^{o}C$ for 12 hours under a vacuum of 10μmHg. This ensures removal of any bound and capillary water adsorbed with the clays, while avoiding irreversible changes to the structure of clays. The degassing temperature of $200^{o}C$ is higher than the API recommended standard of $110^{o}C$ for drying the cores. Luffel and Guidry (1992) suggested a heating temperature of $230^{o}F$ ($110^{o}C$) to remove the free and clay-bound water. Drits and McCarty (2007); Srodon and McCarty (2008) reported that smectite and expandable mixed-layered illite-smectite (I-S) clays are capable of retaining significant electrostatic bound water in excess of $200^{o}C$. They suggested a temperature of $200^{o}C$ to be the optimum for degassing clay rich samples. Figure 2 shows the TGA and DTG curve for Swy-2 heated at the $5^{o}C/min$ rate. The secondary peak in the DTG curve indicates removal of the strongly bound water with clays. We choose a degassing temperature of $200^{0}C$ based on the TGA data and recommendation from Srodon and McCarty (2008).  After

degassing, the sample was exposed to nitrogen gas at liquid nitrogen temperature (-197.26 $^{o}$C) at a series of precisely controlled pressures. Free space (dead volume of the tube) determination was done by volumetrically using helium before measurement of adsorption isotherm. Reagent grade nitrogen and helium (99.99% pure) was used for the experiment. The saturation vapour pressure Po of $N_2$ at 77K was determined every two hours during the experiment using a nitrogen vapor pressure thermometer.

**Mercury Instrusion Capillary Pressure experiment.**

Mercury intrusion experiments were carried on two clay compacted samples using Micromeritics AutoPore IV 9500. The pressure range applied was 0.14-420 MPa with an equivalent pore-size range of 3.6 to$10^4$ nm. The samples are degassed at 50 µmHg evacuation pressure for atleast 30 mins. 3-5 g of samples was used. Every pressure point was equibrated below 0.002 µL/g/s intrusion rate.
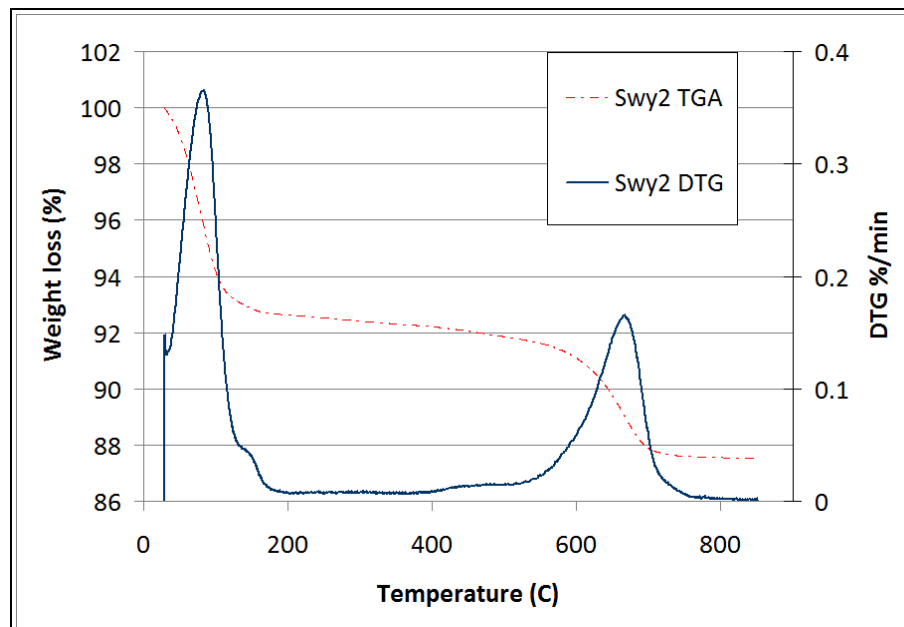


**Figure 2: TGA and DTG curve for Mont-Swy2 powders heated fron 25$^{o}$C -900$^{o}$C at 5$^{o}$/min heating rate. The secondary peak around 160$^{o}$C is related to removal of strong- electrostatically bound water associated with montmorillonite clays. Based on the DTG curve, a degassing temperature of 200$^{o}$C is chosen for our samples**

## Results

### Adsorption Isotherms

Figure 3 shows the adsorption-desorption isotherms of N2 at liquid N2 (77.3K) temperature of 'as-received" powders of Wyoming Montmorillonite Swy-2 and Kaolinite KGa-1b. The isotherms give a qualitative assessment of the porous structure of the materials. Both the isotherms show hysteresis between adsorption and desorption that is characteristic of Type IV isotherms (as per IUPAC classification, Sing 1985). The hysteresis loop is indicative of relative abundance of mesopores where capillary condensation takes place. The hysteresis pattern, termed H3 as per IUPAC classification (Sing, 1985), indicates presence of slit-like pores. The hysteresis effect is more in Swy-2 than in KGa-1b indicating that kaolinite is dominantly macrporous and contains only some mesopores. Volume adsorbed at low P/Po (P/Po<0.01) is indicative of presence of micropores (pore-width < 2 nm). The Wyoming Montmorillonite (Swy-2) has considerable micropores whereas Kaolinite (KGa-1b) has negligible or non-existent micropores. The volume uptake at P/Po near 1.0 indicates the total porosity of materials. Montmorillonite powders have larger porosity than the kaolinite powders. Quantitative estimates of the micropore volume are obtained by t-plots as discussed later.

Figure 4 compares the adsorption-desorption data from the two natural samples: illite-rich Cambrian shale and Niobrara marl B-C. The adsorption isotherms for Swy-2 powder are shown for reference. The porosities of the natural shales are low as compared to the powdered clays as indicated by the volume uptake at high P/Po. Further, the illite-rich Cambrian shale is dominated by micropores while the Niobrara marl B-C does not show significant amount of micropores.
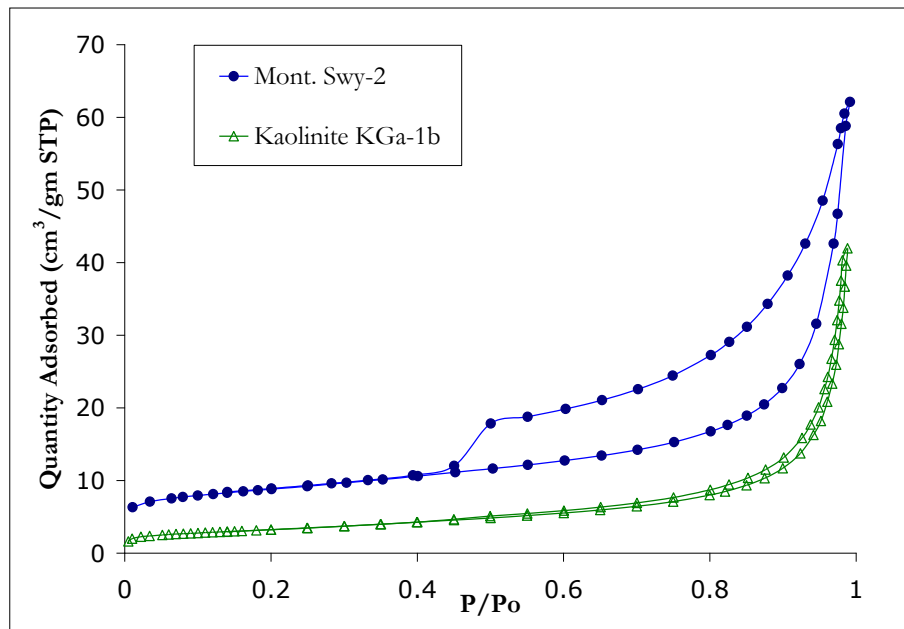
**Figure 3: Adsorption-desorption isotherms of N2 at liquid N2 (77.3K) temperature of 'as-received" powders of Wyoming Montmorillonite Swy-2 and Kaolinite KGa-1b. Both the isotherms show hysteresis that is characteristic of Type IV isotherms. The hysteresis pattern indicates presence of slit-like pores. The hysteresis effect is more in Swy-2 than in KGa-1b indicating that kaolinite is dominantly macrporous and contains only some mesopores. Swy-2 has considerable micropores (pore-width <2 nm) whereas KGa-1b has negligible or non-existent micropores indicated by volume adsorbed at low P/Po (P/Po<0.01). Montmorillonite powders have larger porosity than the kaolinite powders as indicated larger volume uptake at at P/Po near 1.0.**

**Surface Area and Pore volumes:**

We compare here surface areas calculated from the adsorption isotherms using the BET theory and t-plots. We also compare pore volumes obtained from the t-plots and mercury intrusion methods. The aim is to not only characterize the samples but also to understand the source of differences between the methods. One major aspect of this comparison is to understand the contribution of pores smaller than 2 nm (micropores) to total porosity in different shale systems.

The total surface areas of all the samples are obtained from BET theory. The most widely used BET fitting range of P/Po = 0.05-0.30 yields a negetive intercept on the ordinate of the BET transform plot for all of the samples except for kaolinite and Niobrara marl B-C. This is indicative of presence of micropores in the Montmorillonite samples and the illite-rich clays. ISO 9277:2010 recommendations suggest changing the fitting range of BET linear fitting range for microporous materials till a positive intercept is obtained. We followed the modified procedure of applying BET for microporous materials as suggested by ISO 9277:2010. The total surface areas of all the samples are summarized in Table 1. The reporting of BET surface area is done following the recommendations of IS0 9277: 2010

The comparison of BET surface area and t-plot open surface area calculations are given in Table 2. Kaolinite and Niobrara marl B-C show similar surface area obtained from the two methods. Montmorillonite powder Swy-2, pellets made from Swy-2 and illite-rich Cambrian shale show significant difference between the two surface areas. The difference in these values can be correlated to surface area associated with micropores (pore less than 2 nm diameter)  since the 'open surface area' obtained from t-plot typically provides the the surface area from mesopores, macropores, and external surface area (that is the total surface area excluding the surface area of micropores).

Table 3 shows the comparison of the total pore volumes obtained from $N_2$ adsorption isotherm and mercury intrusion with the micropore volume obtained by t-plot method. The total pore volume reported from the $N_2$ adsorption isotherm was calculated by taking the volume uptake at the relative pressure P/Po of 0.98 and using liquid $N_2$ density of 0.808 g/mL. A relative pressure of 0.98 corresponds to a pore-width of 98.78 nm and hence the total pore volume indicated is the pore volume of pores smaller than 98.78 nm diameter. Kaolinite and Niobrara marl B-C show negligible micropore (smaller than 2 nm diameter) volumes. The percentage of micropore volumes to the total pore volume obtained from $N_2$ adsorption isotherm for Montmorrilonite clay samples varies between 7-10%. illite-rich Cambrian shale shows highest proportion of micropores (19.23%) of the total $N_2$ adsorption measured porosity. MICP pore volume for two clays pellets (Mont-4k and Mont10K) shows higher value than the $N_2$ adsorbed pore volume. This difference is attributed to presence of macropores which the $N_2$ adsorption method cannot measure. The MICP however measures pore volume of pores with diameter greater than 3.6 nm. The micropore volumes per unit gram of sample are almost constant for all the montmorillonite clay samples.
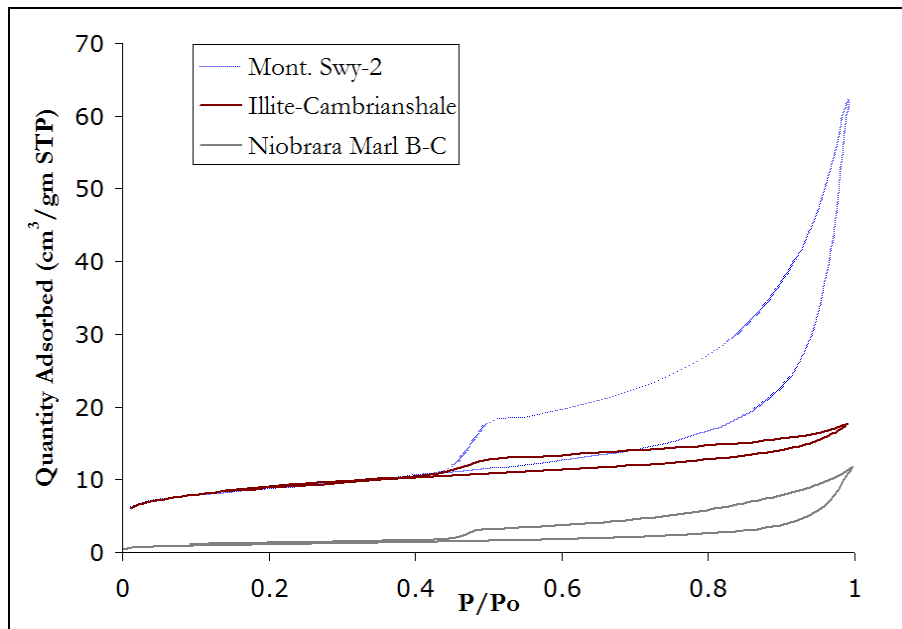
**Figure 4: Adsorption-desorption isotherms of N2 at liquid N2 (77.3K) temperature of illite-rich Cambrian shale and Niobrara marl B-C. Isotherms for Swy-2 are shown for reference. The porosities of the natural shales are low as compared to the powdered clays as indicated by the volume uptake at high P/Po. illite-rich Cambrian shale is dominated by micropores while the Niobrara marl B-C does not show significant amount of micropores indicated by volume adsorbed at low P/Po (P/Po<0.01).**

**Table 1: BET surface area for the samples**

| Sample | Surface Area (m2/g) | C | R2 | Fitting range | |
|---|---|---|---|---|---|
| *As-received Souce Clays (powders)* | | | | | |
| KGa-1b | 11.4869 ± 0.0223 | 158.3 | 0.999980 | 0.0602 | 0.3003 |
| Swy-2 | 31.1325 ± 0.1571 | 1738.0 | 0.999957 | 0.0641 | 0.1623 |
| *Pellets made from Swy-2* | | | | | |
| Mont-4K | 31.8075 ± 0.1606 | 1081.1 | 0.999962 | 0.0645 | 0.1403 |
| Mont-6K | 30.2630 ± 0.1423 | 1231.9 | 0.999967 | 0.0654 | 0.1403 |
| Mont-8K | 31.5500 ± 0.1592 | 1085.9 | 0.999962 | 0.0645 | 0.1408 |
| Mont-10K | 29.7468 ± 0.1310 | 628.7 | 0.999971 | 0.0618 | 0.1408 |
| *Natural shale Samples* | | | | | |
| Niobrara marl BC | 3.8478 ± 0.0081 | 106.9 | 0.999948 | 0.0512 | 0.3039 |
| Cambrian shale | 31.5712 ± 0.1820 | 379.7 | 0.999951 | 0.0379 | 0.1809 |

**Table 2: Comparison of BET surface area, open surface area obatined from t-plot and micropore surface area of the samples based on N2 adsorption isotherms**

| Sample | BET Surface Area (m2/g) | Open Surface Area by t-plot (m2/g) | % Surface area contributed by micropores (%) |
|---|---|---|---|
| *As-received Souce Clays (powders)* | | | |
| KGa-1b | 11.49 | 11.40 | 0.78% |
| Swy-2 | 31.13 | 19.68 | 36.78% |
| *Pellets made from Swy-2* | | | |
| Mont-4K | 31.81 | 18.73 | 41.12% |
| Mont-6K | 30.26 | 17.71 | 41.47% |
| Mont-8K | 31.55 | 18.50 | 41.36% |
| Mont-10K | 29.75 | 18.26 | 38.62% |
| *Natural shale Samples* | | | |
| Niobrara marl BC | 3.84 | 3.80 | 1.04% |
| Cambrian shale | 31.57 | 20.93 | 33.70% |

**Table 3: Comparison of total and micropore volumes of the samples determined by N2 adsorption data by t-plot and Hg-porosimetry**

| Sample | Total Pore Volume N2 (cc/g) | Total Pore Volume Hg-porosimetry (cc/g) | Micropore volume by t-plot (cc/g) | % Micropore |
|---|---|---|---|---|
| KGa-1b | 0.049 | -- | 0.000 | 0.00 % |
| NaM100-pw-US | 0.068 | -- | 0.005 | 7.35 % |
| Mont-4K | 0.063 | 0.206 | 0.006 | 9.52 % |
| Mont-6K | 0.060 | -- | 0.005 | 8.33 % |
| Mont-8K | 0.062 | -- | 0.006 | 9.68 % |
| Mont-10K | 0.056 | 0.129 | 0.005 | 8.93 % |
| Niobrara marl BC | 0.014 | -- | 0.000 | 0.00 % |
| illite-Cambrian shale | 0.026 | -- | 0.005 | 19.23 % |

**Pore-Size Distributions:**

Source Clays: Figure 5 shows the pore size distribution [partial volume V of each pore diameter D, dV/dlog(D)] obtained from the adsorption  isotherm curves for the powdered source clay samples. The parameter dV/d(logD) is used because the area under the curve between any two pore diameters can be used to assess the partial porosity for each pore diameter range.  For montmorillonite powder Swy2, the distribution is bimodal, a major peak between 60-100 nm with a minor peak around 3-4 nm. Kaolinite KGa-1b shows mostly a unimodal pore distribution with peak around 100 nm.

Compaction: Figure 6 shows the pore-distributions of the compacted pellets made from Swy-2. The compacted pellets show similar bimodal pore-size distribution as the powder Swy-2. The pore volume around 3-4 nm peak does not change with the applied axial load. There is a significant decrease in pore volume in the compacted pellets around the 60 nm peak with the greatest decrease seen between Swy2 powder and pellets compacted at 4000 psi (Mont-4K). With further compaction there is a slight decrease in porosity in 60 nm range. The pore-size distribution patterns are consistent for all the compacted pellets. Figure 7 shows the pore-size distribution curves obtained for MICP on Mont-4K and Mont-10K.  It shows a dominant bimodal dritribution with modes at 20nm and around 1000-2000 nm. The porosity around 1000-2000 nm decreases with compaction, Mont-4K have larger pore volume in that pore range compared to Mont-10K. Also the mode decreases from 2000 nm in Mont-4k to 1000 nm in Mont-10K. There is a minor peak around 4 nm but with the current resolution, we cannot distinguish the data from noise.

Natural shales: Figure 8 show the pore-size distribution of the natural samples obtained from $N_2$ adsorption isotherms. The Cambrian shales is dominated by micropores (with diameter around 2-3 nm) while contribution of such micropores is insignificant in Niobrara marl B-C.
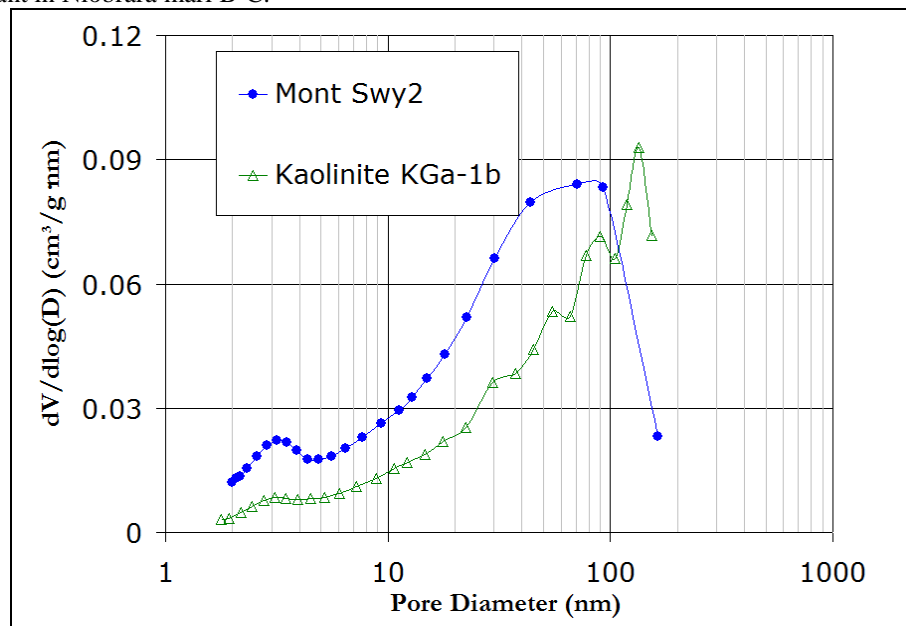


**Figure 5: Pore-size distribution of 'as-received' source clay powders: Wyoming Montmorillonite (Swy2) and Georgia Kaolinite (KGa-1b) obtained from N2 adsorption isotherm. Swy2 have bimodal distribution with a major peak between 60-100 nm with a minor peak around 3-4 nm. KGa-1b shows unimodal pore distribution with peak around 100 m.**
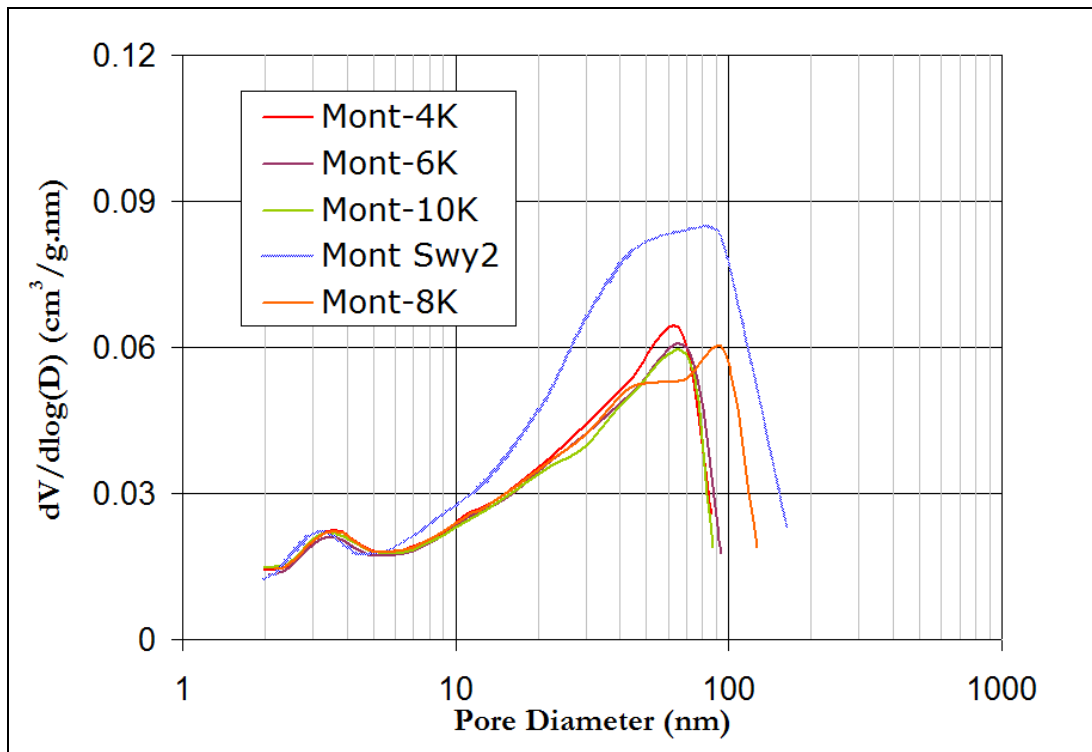
**Figure 6: Pore-size distribution of compacted clay pellets obtained from N2 adsorption isotherm. The samples were named using clay mineral identifier and the pressure applied, e.g. sample Mont-6K means the pellet is made from Wyoming Montmorillonite by applying 6K psi of axial load. The samples show similar consistent bimodal pore-size distributions as Swy-2. Pore volume around 3-4 nm peak remain unchanged with the applied axial load. There is a significant decrease in pore volume in the compacted pellets around the 60 nm peak with the greatest decrease seen between Swy2 powder and pellets compacted at 4000 psi (Mont-4K). With further compaction there is a slight decrease in porosity in 60 nm range. The pore-size distribution patterns are consistent for all the compacted pellets.**
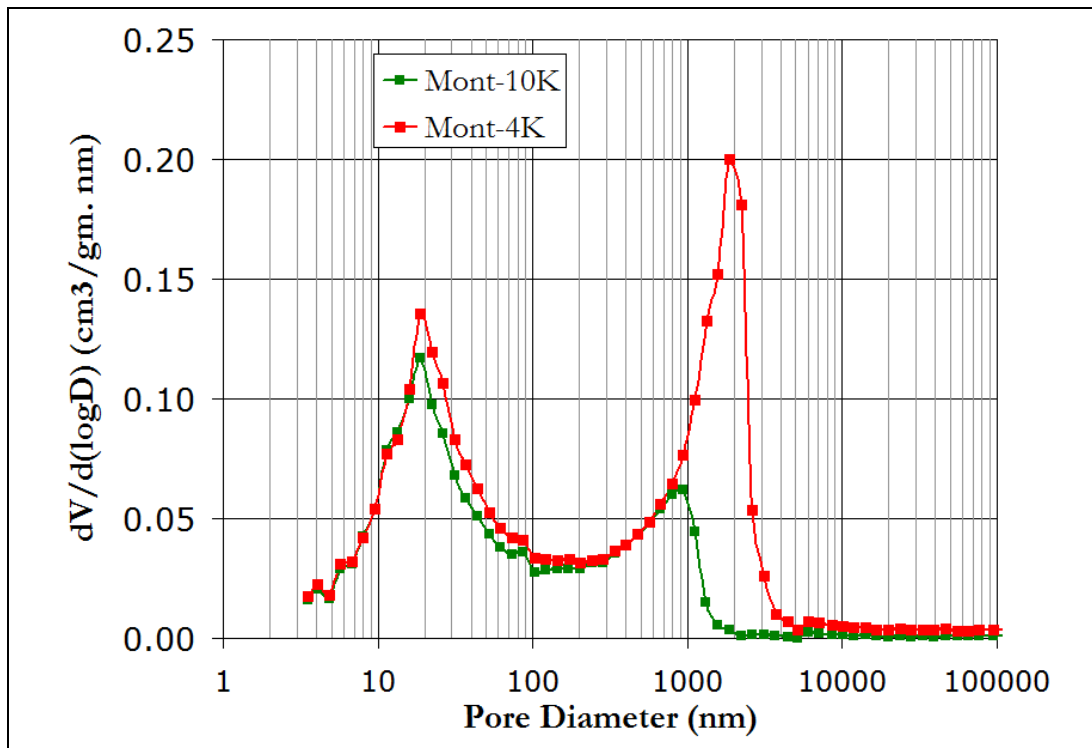


**Figure 7: Pore-size distribution of compacted clay pellets Mont-4k and Mont-10K obtained from Hg-porosimetry. Bimodal dritribution with modes at 20nm and around 1000-2000 nm are observed. Pore volume around 1000-2000 nm decreases with compaction. Also the mode decreases from 2000 nm in Mont-4k to 1000 nm in Mont-10K. There is a minor peak around 4 nm but cannot be distinguised from noise.**
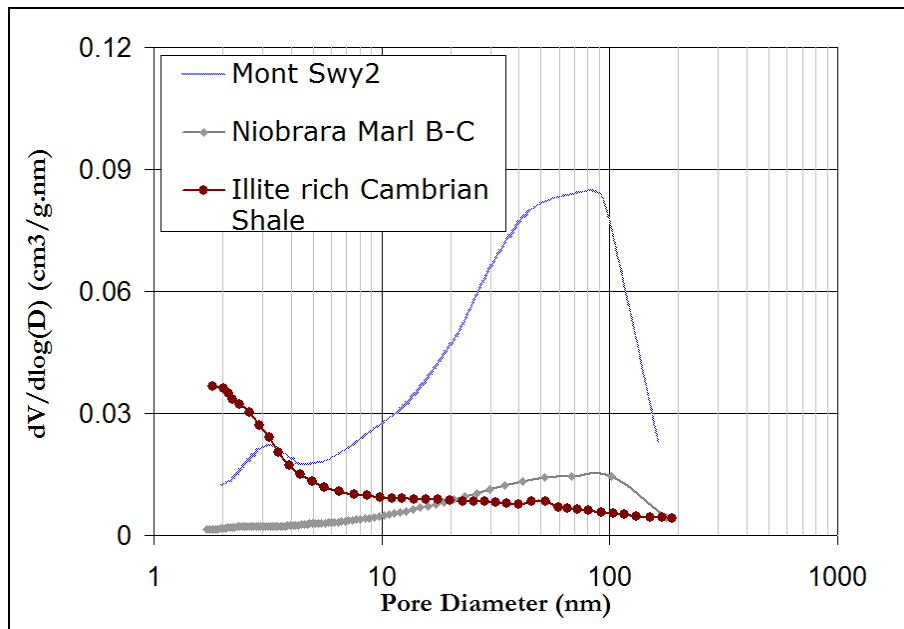
**Figure 8: Pore-size distribution of illite-rich Cambrian shale and Niobrara marl B-C obtained from N2 adsorption isotherm. The pore-size distribution of Swy-2 is shows as reference. The Cambrian shales is dominated by micropores (with diameter around 2-3 nm) while contribution of such micropores is insignificant in Niobrara marl B-C.**

**Discussion:**

The measured surface area of the source clays Swy2 and KGa-1b (31.13 and 11.49 $m^2/g$, respectively) is in good agreement with the reported values by the Clay Mineral Society (31.82 and 10.4 $m^2/g$, respectively) (http://www.clays.org/SOURCE%20CLAYS/SCdata.html). For the compacted pellets, surface area does not show a definitive trend with compaction (Figure 9). The pore volume for pores with diameter less than 98.78 nm decreases with compaction except for Mont-8k. The pore volume is highest in the powder and it decreases with compaction. This agrees with the observed compaction curves where porosity of shales decreases with compaction. Note that probably due to sample preparation problems, Mont-8k deviates from the general compaction trend having higher pore volume then less compacted Mont-6K. Mont-8K's pore-size distribution is also slightly different fron rest of the compacted pellets.

The presence of micropores (< 2 nm) agrees well with the results of homoionic pure Wyoming montmorillonite (Rutherford et al., 1997). The reported micropore volumes, between 0.004-0.008 cc/g for different exchange cations, lies in the range of our measured micropore volumes for natural untreated montmorillonite (0.006 cc/g). The micropore volume does not change with compaction suggesting that micropores are shielded from compaction.

The pore-size distribution curves from $N_2$ adsorption and MICP shows good correlations. $N_2$ adsorption isotherm gives pore-size distribution information from 1.7 – 100 nm pore diameter whereas MICP experiments give pore information between 3.6nm -1000 µm pore diameter. However, concerns remain on the validity of high pressure data obtained from the MICP experiments. Our results show good correlation between the pore size distribution of $N_2$ adsorption and mercury intrusion (Figure 10). The modes detected at 3-4 nm and around 60-70 nm is also observed in MICP experiments, although the position of the peaks does not match precisely. MICP suggests a lower pore–diameter (20 nm). This may be due the compressibility of grains at high mercury instrusion pressure resulting in underestimation of pore diameter. The pore-size distribution suggests multiple scale of porosity associated with clays. Aylmore and Quirk (1967) and Julian et al. (2005) have reported the multiscale porosity associated with clay structures, especially with montmorillonites. The pore-size distribution peaks in clays can be correlated with their intra-particle and inter-particle porosity. Pores with diameter between 10 to 100 nm are dominant in the pore spaces between bundles of clay platelets (inter-particle porosity) while pores with diameter account for the porosity within one bundle of clay platelets (intra-particle porosity). The mode around 2000 nm obtained from the MICP data can be correlated with the macropores between the aggregates of clays. Compaction has the biggest effect on the macropores. With increasing axial pressure, the pore volumes around 2000 nm is affected most and also the mode shifts to lower pore-sizes. This can be attributed to better alignment of clay particles and compaction of pore with applied stress. The intermediate mode is less affected from compaction whereas the intra-particle porosity (pores with 3-4 nm diameter) remains constant with compaction. This intra-particle porosity is shielded from the effect of compaction and is speculated to exist in all clay-rich shales irrespective of their burial depth. This has important implications for storage capacity of shale reservoirs. Prasad and Bryar (2003) found the significance of intermediate pore sizes (20-30 µm) in seismic studies of clay cements: as soon as kaolinite powders were dried such that they only had water in pore sizes around 20 µm, kaolinite was found to give shear strength to two quartz discs. The shear wave signal increased by about an order of magnitude.
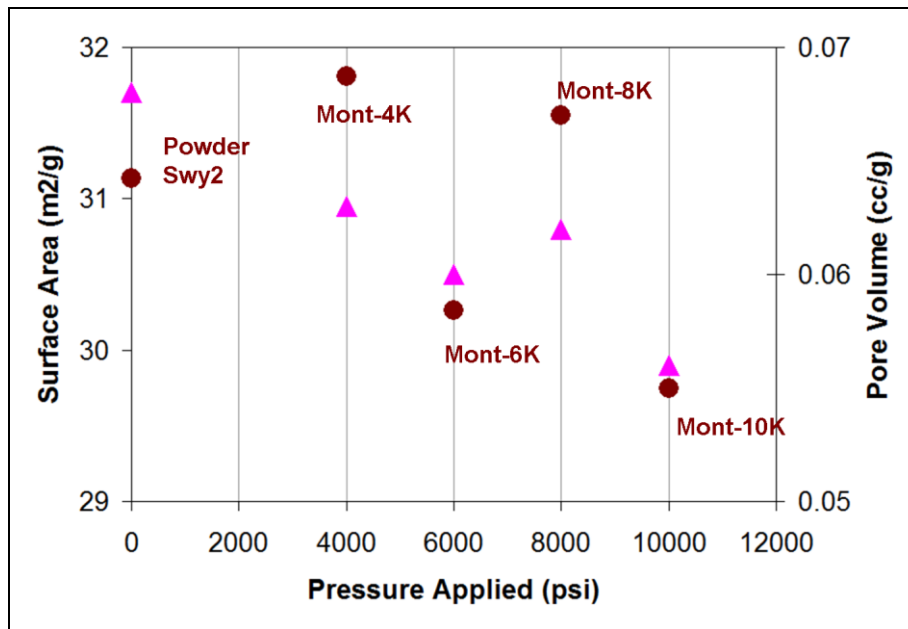
**Figure 9: Surface Area (circle) and Pore-volume for pores with diameter less than 98.78 nm (triangle) of the compacted pellets with increasing axial load. Surface area does not show a definitive trend with compaction. The pore volume decreases with compaction except for Mont-8k. The pore volume is highest in the powder and it decreases with compaction. Note that probably due to sample preparation problems, Mont-8k deviates from the general compaction trend having higher pore volume**
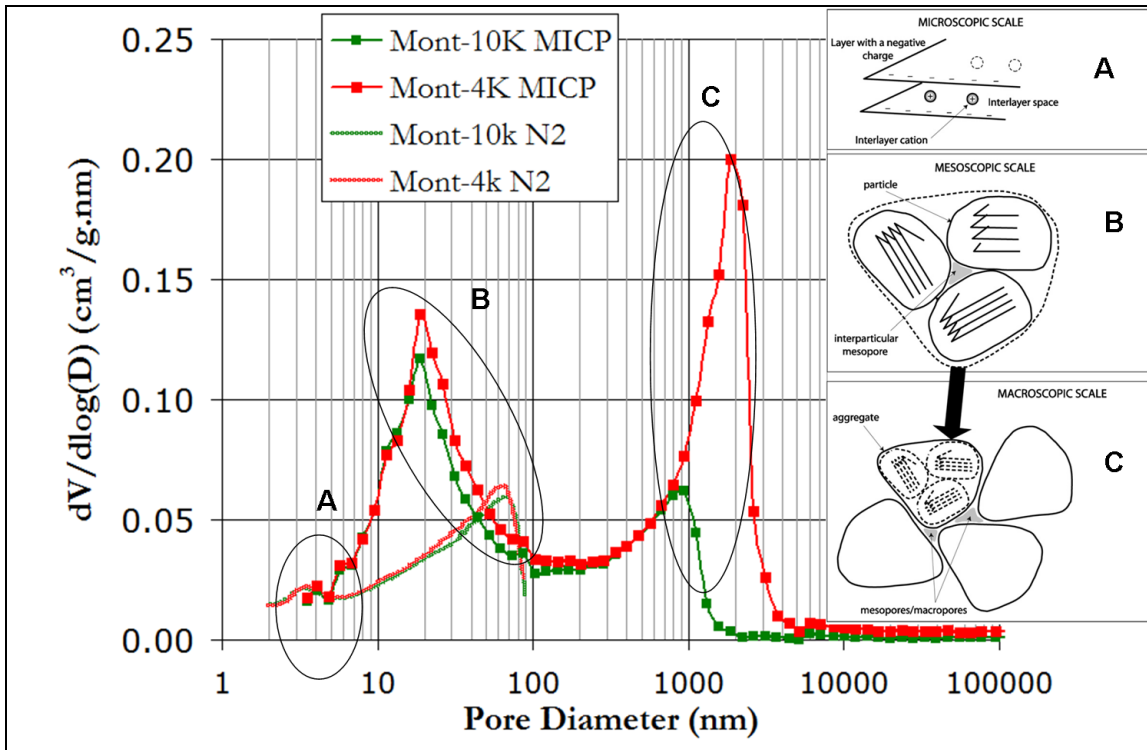


**Figure 10: Comparison of the pore size distribution of N2 adsorption and mercury intrusion porosimetry for Mont-4K and Mont-10K. The modes detected at 3-4 nm and around 60-70 nm in N2 is also observed in MICP experiments, although the position of the peaks does not match precisely. MICP suggests a lower pore–diameter (20 nm) which may be due to compressibility of grains at high mercury instrusion pressure leading to underestimation of pore diameter. The three modes obserbed in pore-size distribution can be correlated with multi-scale porosity associated with clay structures especially montmorillonites (See Insert, From Jullien et al. 2005). Mode A corresponds to interlayer and intra-particle pores, Mode B corresponds to inter-particular mesopore and Mode C corresponds to macropores between aggregates.**

**Table 4: Summary of pore space characterization results from gas adsorption and mercury injection, and mineralogy. Note informations on macropores are not available (n/a) for samples since Hg-porosimetry was not run on those specific samples**

| Sample | Source | Mineralogy | Micropores | Macropores | PSD |
|---|---|---|---|---|---|
| KGa-1b | Source clay | Pure Kaolinite | No | n/a | Unimodal: 100 nm |
| NaM100-pw-US | Source clay | Pure Mont | Yes | n/a | Bimodal: 3; 60 nm |
| Mont-4K | Source clay | Mont at 4kpsi | Yes | Yes | Bimodal: 3; 60 nm |
| Mont-6K | Source clay | Mont at 6kpsi | Yes | n/a | Bimodal: 3; 60 nm |
| Mont-8K | Source clay | Mont at 8kpsi | Yes | n/a | Bimodal: 3; 60 nm |
| Mont-10K | Source clay | Mont at 10kpsi | Yes | Yes | Bimodal: 3; 60 nm |
| Niobrara marl BC | Natural marl | Calcite rich, little clay | No | n/a | Unimodal: 90 nm |
| Illitic Cambrian shale | Natural shale | Illite-rich siliceous shale | Yes | n/a | Unimodal, 2-3 nm |

Our results from the various measurements are summarized in Table 4. The pore-size distribution of Niobrara marl B-C and illite-rich Cambrian shale reveals difference in pore-structure in shales based on the difference in mineralogy. Niobrara marl B-C is a calcite rich lithology with about 20-30% illitic-smectitic clays while the Cambrian shale is a illite dominated siliceous shale. The presence of micropores in illite-rich Cambrian shale and absence of micropores in Niobrara marl B-C can be attributed to the relative abundance of clay minerals in the former. The dominant pore size for illite-rich Cambrian shale is aroung 2-3 nm and this can be interpreted as the shielded intra-particle porosity associated with clay minerals. The relative dominance of micropores in illite-rich Cambrian shale makes it better candidate for gas-adsorption potential than Niobrara marl B-C. Right now, the gas-adsorption potentials of these shales is only a speculation and need to be validated by experimental results with high-pressure gas sorption experiments. Further studies are being done along this line to investigate this phenomena in details.

## Conclusions

We recommend that using a combined experimental technique including $N_2$ gas adsorption technique and Hg-porosimetry to investigate the full sprectrum of pore structure in clays and shales. Our results on pure clay minerals and natural shales show that

- clays have a mulit-scale pore-structure at different dimensions
- Depending upon mineralogy, micropores are associated with clays. For example, Micropores are associated with montmorillonite clays but not with kaolinite
- Clays, especially montmorillonite, show multiple scales of pore-structures corresponding to intra-particle porosity with bundles of clay platelets, inter-particle mesopores between each clay bundles and macropores between the aggregates of clays.
- Compaction results in decrease in pore volume and reduction of pore-size in the macropores of the clays while the micropores are shielded from the effect of compaction
- In natural shales, mineralogy controls the pore-size distributions for shales and presence of micropores in natural shales can be correlated with the dominance of illite-smectite type of clays in the rock.

## Acknowledgments

## References

Aylmore, L.A.G., and Quirk, J.R., 1967, The micropore size distribution of clay mineral systems. J Soil Sci, **18**, 1-17.

Bustin, R., Bustin, A., Cui, X., Ross, D. and Pathi, V. M., 2008, Impact of shale properties on pore structure and storage characteristics: SPE Paper No 119892, Presented at the SPE Shale Gas Production Conference, Society of Petroleum Engineers, Fort-Worth, USA, 16-18 November

Connell-Madore, S. and Katsube, T.J., 2006, Pore-size-distribution characteristics of Beaufort-Mackenzie Basin shale samples, Northern Territories, Geological Survey of Canada, Current Research, **2006-B1**, 18p.

Clay Mineral Society Source Clay Information: http://www.clays.org/SOURCE%20CLAYS/SCdata.html

Diamond, S., 1970, Pore size distributions in clays: Clay and Clay Minerals, **18**, 7-23.

Drits, V. A. and McCarty, D. K., 2007, The nature of structure-bonded $H_2O$ in illite and leucophyllite from dehydration and dehydroxylation experiments: Clays and Clay Minerals, **55**, 45-58.

Ewy, R. T. and Morton, E. K., 2009, Wellbore-stability performance of water-based mud additives: SPE Drilling and Completion, **24**, 390-397.

Groen, J.C., Peffer, L.A.A. and Perez-Ramırez, J, 2003, Pore size determination in modified micro- and mesoporous materials. Pitfalls and limitations in gas adsorption data analysis, Microporous and Mesoporous Materials, **60** , 1–17

ISO 9277:2010, 2010, Determination of the specific surface area of solids by gas adsorption -- BET method.

Jaffe, A., 2010, Shale gas will rock the world: Retrieved January 26, 2011, from The Wall Street Journal: http://online.wsj.com/article/ SB10001424052702303491304575187880596301668.html.

Javadpour, F., 2009, Nanopores and apparent permeability of gas flow in mudrocks (shales and siltstone): Journal of Canadian Petroleum Technology, **48**, 16-21.

Jullien, M., Raynal, J., Kohler, E. and Bildstein, O., 2005, Physicochemical reactivity in clay rich materials: tools for safety assessment, Oil and Gas Science Technology, **60 (1)**, 107–120

Loucks, R. G., Reed, R. M., Ruppel, S. C. and Jarvie, D. M., 2009, Morphology, genesis, and distribution of nanometer-scale pores in siliceous mudstones of the Mississippian Barnett Shale: Journal of Sedimentary Research, **79**, 848-861.

Luffel, D. L. and Guidry, F. K. 1992, New core analysis-methods for measuring reservoir rock properties of devonian shale: Journal of Petroleum Technology, **44**, 1184-1190.

Pollastro, R.M., 1992, Natural fractures, composition, cyclicity, and diagenesis of the Upper Cretaceous Niobrara Formation, Berthoud field, Colorado, in Schmoker, J.W., Coalson, E.B., and Brown, C.A., eds., *Geological Studies Relevant to Horizontal Drilling: Examples from Western North America*: Rocky Mountain Association of Geologists, p. 243-255.

Prasad, M., Bryar, T, 2003, Clay in Contact Zones: NMR and Ultrasonic Effects: Eos Trans. AGU, 84(46), Fall Meet. Suppl., Abstract H12H - 08.

Ross, D.J.K., and Bustin, R.M., 2009, The importance of shale composition and pore structure upon gas storage potential of shale gas reservoirs, Marine and Petroleum Geology, **26**, Issue 6, 916-927.

Rutherford, D.W., Chiou, C.T. and Eberl, D.D. 1997, Effects of exchanged cation on the microporosity of montmorillonite, Clays and Clay Minerals,  **45**, 534-543.

Sing, K. S., 1985, Reporting physisorption data for gas/solid systems with special reference to the determination of surface area and porosity: Pure and Applied Chemistry, **57**, 603-619.

Srodon, J. and Eberl, D.D., 1984. Illite. In: S.W. Bailey (Editor), *Micas. Reviews in Mineralogy*, **13,** Mineralogical Society of America

Srodon, J. and McCarty, D. K.  2008, Surface area and layer charge of smectite from CEC and EGME/ $H_2O$-retention measurements: Clays and Clay Minerals, **56**, 155-174.

Webb, P.A. and Orr, C., 1997, *Analytical Methods in Fine Particle Technology*, Micromeritics Instrument Corporation, Norcross, GA, USA.